

Whole Skin Locomotion Inspired by Amoeboid Motility Mechanisms: Mechanics of the Concentric Solid Tube Model

By
Mark Edward Ingram

Thesis submitted to the faculty of the Virginia Polytechnic Institute and State
University in partial fulfillment of the requirements for the degree of
Master of Science
In
Mechanical Engineering

Dr. Dennis Hong, Committee Chair
Dr. Charles Reinholtz
Dr. Robert Sturges

August 10, 2006
Blacksburg, Virginia

Keywords: Whole Skin Locomotion, Biomimetic, Robotics, Amoeba

Copyright 2006, Mark E. Ingram

Whole Skin Locomotion Inspired by Amoeboid Motility Mechanisms: Mechanics of the Concentric Solid Tube Model

Mark E. Ingram

ABSTRACT

As the technology of robotics intelligence advances, and new application areas for mobile robots increase, the need for alternative fundamental locomotion mechanisms for robots that allow them to maneuver into complex unstructured terrain becomes critical. In this research we present a novel locomotion mechanism for mobile robots inspired by the motility mechanism of certain single celled organisms such as amoebae. Whole Skin Locomotion (WSL), as we call it, works by way of an elongated toroid which turns itself inside out in a single continuous motion, effectively generating the overall motion of the cytoplasmic streaming ectoplasmic tube in amoebae.

This research presents the preliminary analytical study towards the design and development of the novel WSL mechanism. In this thesis we first investigate how amoebas move, then discuss how this motion can be replicated. By applying the biological theories of amoeboid motility mechanisms, different actuation models for WSL are developed including the Fluid Filled Toroid (FFT) and Concentric Solid Tube (CST) models. Then, a quasi-static force analysis is performed for the CST model and parametric studies for design, including power efficiency and force transition characteristics, are presented.

Acknowledgments

I would like to acknowledge the following people for their help in my graduate work:

Dr. Dennis Hong, my advisor, for his tireless efforts, while simultaneously working on many projects, including setting up RoMeLa (the Robotics and Mechanisms Laboratory). Working for him has been a great experience.

Mrs. Hong, for her patience when I monopolize her husbands time.

My thesis committee, Dr. Charles Reinholtz and Dr. Robert Sturges for their time and useful insights into the problem of Whole Skin Locomotion.

Mark Showalter for his work on the feasibility experiments, and all of my lab colleagues for their assistance and sense of fun.

Dr. Harry Robertshaw and Dr. Michael Alley for hiring me a TA for multiple semesters, and there guidance during that period of time.

Dr. Bob Williams of Ohio University for his mentorship during my undergraduate career, and pointing me towards Virginia Tech.

And finally my parents for their constant support throughout my life, without which none of this would be possible.

Table of Contents

ABSTRACT	ii
Acknowledgments	iii
Table of Contents	iv
Table of Figures	v
Chapter 1: Introduction	1
Chapter 2: Biologically Inspired Whole Skin Locomotion	3
Chapter 3: Theories of Amoeboid Motility Mechanisms	5
3.1 TAIL CONTRACTION	5
3.2 FRONTAL-ZONE CONTRACTION	6
Chapter 4: Models for the Whole Skin Locomotion Mechanism	7
4.1 REAR CONTRACTILE RINGS WITH CST	8
4.2 FRONTAL EXPANSILE RINGS WITH CST	8
4.3 WAVE CONTRACTILE/EXPANSILE RINGS WITH CST	9
4.4 REAR SKIN CONTRACTION WITH FFT	9
4.5 ACTUATION METHODS AND PACKAGING	10
Chapter 5	13
Feasibility Experiments	13
5.1 FEASIBILITY EXPERIMENT WITH PRE-TENSIONED ELASTIC SKIN	13
5.2 REAR SKIN CONTRACTION EXPERIMENT USING TENSION CORDS.....	14
Chapter 6: Analysis of the CST Model	16
NOMENCLATURE	16
6.1 MECHANICS OF A SINGLE ACTUATION RING OVER A CST	17
6.1.1 <i>Region I</i>	18
6.1.2 <i>Region II</i>	20
6.1.3 <i>Region III</i>	24
6.1.4 <i>Region IV</i>	24
6.2 MECHANICAL ADVANTAGE AND EFFICIENCY FOR DIFFERENT CROSS-SECTION GEOMETRIES.....	24
6.2.1 <i>Round Cross-section, Region I</i>	25
6.2.2 <i>Straight Line Cross-section, Region I</i>	27
6.2.3 <i>Composite Cross-section, Region I</i>	29
6.2.4 <i>Region II</i>	32
6.2.5 <i>Region III and IV</i>	34
6.3 ANALYSIS AND SIMULATION FOR THE CST MODEL SYSTEM	34
6.3.1 <i>Displacement Constraints of the Actuation Rings for the CST Model System</i>	34
6.3.2 <i>Input Tension Required for the Actuation Rings for the CST Model System</i>	35
Chapter 7: Conclusions and Future Work	38
References	40

List of Figures

Figure 1. Amoeba proteus and its pseudopods.	2
Figure 2. Motility mechanism of a monopodial amoeba.	3
Figure 3. Unique mobility of a robot using WSL.	4
Figure 4. Motion generated by the rear contractile rings (1a, 2a, 3a) and frontal expansile rings (1b, 2b, 3b) for the concentric solid tube (CST) model.	7
Figure 5. Larger-scale actuation strategies.	10
Figure 6. Smaller-scale actuation strategies with EAP.	10
Figure 7. One possible example for component packaging; the “dog bone” concept.	12
Figure 8. Construction of a pre-tensioned elastic skin FFT model and its energy states.	13
Figure 9. Motion of the pre-tensioned elastic-skin FFT model.	14
Figure 10. Sequence of pictures of the locomotion of the pre-tensioned elastic-skin model.	14
Figure 11. Sequence of pictures of the tension cord actuated model locomotion.	15
Figure 12. Free body diagram of a contracting ring actuator.	17
Figure 13. The four active and two passive regions of the straight line with round edge CST. ...	18
Figure 14. Free body diagram of a membrane segment between the contractile ring and region I of the CST.	19
Figure 15. The three modes of operation in region II, fully in contact (mode 1), partially in contact (mode 2), and no contact (mode 3).	20
Figure 16. Free body diagram of multiple actuating rings in Region II.	21
Figure 17. The actuation ring in Region II as a three-force member.	22
Figure 18. Mechanical advantage and efficiency versus percent of travel for a circular cross-section CST in Region I with varying friction coefficients.	26
Figure 19. Mechanical advantage and efficiency of a strait line cross-section CST, for varying friction and a constant slope angle of 45°	28
Figure 20. Mechanical advantage and efficiency of a strait line cross-section CST, for varying slope angles and a friction coefficient of 0.	28
Figure 21. Composite cross-section CST.	29
Figure 22. Mechanical advantage and efficiency for a composite cross-section CST with varying friction coefficients.	30
Figure 23. Mechanical advantage and efficiency for a composite cross-section CST with varying slope angles.	30
Figure 24. Mechanical advantage and efficiency for a composite cross-section CST with varying geometry.	31
Figure 25. Mechanical advantage of the round cross-section, region II, mode 3, with unit ring tensions, and varying ring spacing.	33
Figure 26. Ring radius versus position for a single ring over a circular cross-section CST.	35
Figure 27. Tension input required in region I, for a unit force output, frictionless.	36
Figure 28. Tension input required for a unit force output.	37

Chapter 1

Introduction

As the technology of robotics intelligence advances, and new application areas for mobile robots increase, the need for alternative fundamental locomotion mechanisms for robots that can enable them to maneuver into complex unstructured terrain becomes critical. Current methods of ground vehicle locomotion are based on wheels, tracks or legs, and each of these methods has its own strengths and weaknesses [1, 2, 3]. In order to move a robot into an area of complex terrain a new method of locomotion is needed. For example, to be able to find people trapped in a collapsed building, a robot would need to be able to move over, under and between rubble, and maneuver itself into tight corners. Current methods of locomotion can do some part of this, but they have only had limited success in achieving all of these capabilities [4, 5].

In this research we present a novel locomotion mechanism for mobile robots inspired by the motility mechanism of certain single celled organisms such as amoebae (Figure 1). The Whole Skin Locomotion (WSL) [6], as we call it, works by way of an elongated toroid which turns itself inside out in a single continuous motion, effectively generating the overall motion of the cytoplasmic streaming ectoplasmic tube in amoebae. The unique mobility of WSL makes this the ideal locomotion method for search-and-rescue robots that need to traverse over or under rubble [7, 8], or for medical applications such as robotic endoscopes where a robot needs to maneuver itself into tight spaces [9, 10, 11]. The WSL is a new class of mechanism [12] that generates an everting motion from the expanding and contracting motion of actuators that, if successful, will also enable smart materials such as electroactive polymers to be used in ways not possible before, opening the door for them to be used in new and exciting applications [13, 14, 15].

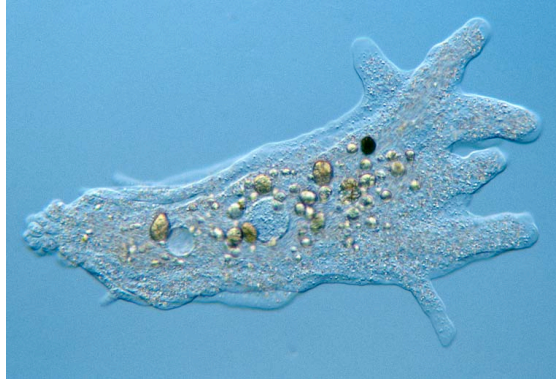


Figure 1. Amoeba proteus and its pseudopods.

The goal of this research was to investigate this new method of locomotion, and here we present the preliminary analytical study towards the design and development of the novel WSL mechanism. Two methods of replicating this everting toroidal motion have been proposed. The first is the Fluid Filled Toroid (FFT) model, and the second is the Concentric Solid Tube (CST) model. The feasibility of this new way of moving is demonstrated, and the mechanics of the CST model are studied. The proposed actuation method for WSL is expanding and contracting ring actuators. This research focuses on the mechanics of the rings as they move around the CST by performing a quasi-static force analysis and parametric study for design, including power efficiency and force transition characteristics.

Chapter 2

Biologically Inspired Whole Skin Locomotion

Single celled organisms have three primary ways of locomotion; using flagella, cilia, or pseudopods [16]. A flagellum is a single tail that drives itself like that of a tadpole, and cilia are small hair-like strands that are used for swimming or crawling. A pseudopod is part of a cell that extends itself, similar to a leg (Figures 1 and 2). Pseudopods form by a process called cytoplasmic streaming, a process in which endoplasm flows forward inside the ectoplasmic tube to protrude the pseudopod tip outward of the body [16, 17] as shown in Figure 2.

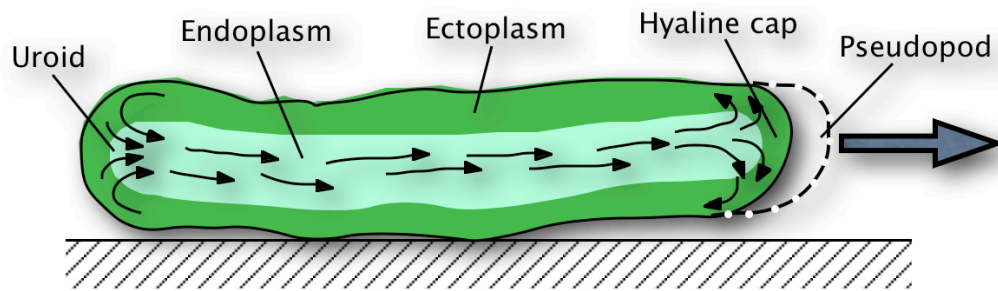


Figure 2. Motility mechanism of a monopodial amoeba.

The name “Whole Skin Locomotion” comes from the fact that the entire outer surface of a robot using this locomotion mechanism is used as a surface for traction and that the entire skin is used for the actuation by cycling through contractions and expansions to generate an everting motion [6]. This is fundamentally different from the undulatory motion of snakes [7, 18, 19] or inchworms [20, 21], as WSL works more like a three-dimensional tank tread. Since the entire skin is used for locomotion, the robot can move as long as any surface of the robot is in contact with the environment, be it the ground, walls or obstacles on the side, or the ceiling. With an elastic membrane or a mesh of links acting as its outer skin, the robot can easily squeeze between obstacles or under a collapsed ceiling and move forward using all its contact surfaces for traction (Figure 3(a)), or even squeeze itself through holes with diameters smaller than its nominal width (Figure 3(b)). This makes WSL the ideal locomotion method for search-and-rescue robots, medical robots [22, 23, 24], or robots for inspecting gas pipes for corrosion and leakage [25].

Especially for robotic endoscope applications, since the very delicate gastrointestinal tract has sharp turns and changes in diameter [9], WSL could be used to minimize the possibility of damage to a person as it distributes the force required for movement over the largest possible area and morphs its shape to match that of the gastrointestinal tract.



(a) Squeezing under a ‘collapsed ceiling’ using all surfaces for traction



(b) Passing through a hole smaller than half the size of its nominal diameter

Figure 3. Unique mobility of a robot using WSL.

Some examples of robots that use the idea of distributed contact locomotion include the rolling stent endoscope [26] and a cylindrical robot with feet distributed over the surface [27, 28]. The rolling stent endoscope uses a “rolling donut” constructed from three stents positioned around the endoscope tip for intestinal locomotion, and the cylindrical robot with distributed feet performs a coordinated shoveling motion of the feet that provides forward propulsion wherever a foot is in contact with any feature in the environment. Another example is a mono-tread robot [29] that uses a steerable single continuous belt. In a sense, all of these robots share some similar characteristics with WSL; however, their topology and method of actuation are completely different.

Chapter 3

Theories of Amoeboid Motility Mechanisms

Among the many theories of amoeboid motility mechanisms proposed by biologists [16, 17, 30], we will be applying two theories we consider the most useful to adapt and implement for the WSL actuation models. These are the tail contraction model and the frontal-zone contraction model.

In both models, the motion of the body is caused by the process of cytoplasmic streaming (Figure 2). Cytoplasm is made up of gel-like ectoplasm and liquid endoplasm. The endoplasm flows forward inside the ectoplasmic tube, which acts as the outer skin. When the endoplasm reaches the front, it turns into the gel-like ectoplasm forming the pseudopodial tip in a region called the hyaline cap. The pseudopodial tip in turn forms an extension of the ectoplasmic tube, moving the organism forward. As the amoeba advances, the ectoplasmic tube turns into the liquid endoplasm at the rear, or uroid of the cell, and the process continues [16, 17]. The net effect of this ectoplasm-endoplasm transformation is the forward motion of the amoeba.

Most researchers in the field agree that the motor for the motion of the amoeba is actomyosin based. Actomyosin is a protein complex in muscle fibers composed of myosin and actin. It shortens when stimulated and causes muscle contractions in biological systems [16, 17, 31]. Exactly how the actomyosin based cytoplasmic streaming happens is still debated, and many theories exist; however, the tail contraction model and the frontal-zone contraction model are the two theories we apply to the WSL mechanism model.

3.1 Tail Contraction

The tail contraction model, first put forward by Ecker [32, 33], is based on the observable contraction of the rear of the cell. While the amoeba is moving, the membrane around the uroid, or tail, folds up because the ectoplasm immediately under it is turning into endoplasm. The idea is that as the tail contracts, it causes a small positive pressure within the cytoplasm which would force more fluid endoplasm forward along the line of least resistance. This theory was supported by basic observations of a moving amoeba, and in experiments where particles implanted in the cytoplasm come closer together in the uroid, indicating contraction of the cytoplasm [34]. The

pressure gradient caused by the contraction can be measured by having an amoeba crawl through a hole between two chambers and measuring the pressure difference [16].

3.2 Frontal-Zone Contraction

The frontal-zone contraction model proposes to explain the mechanism by the assembly process of endoplasm into gel-like ectoplasm at the advancing tip of the pseudopod, accompanied by contraction, pulling the endoplasm forward and pushing the pseudopod tip outward. This theory was proposed after an experiment in 1960 which could not be explained by the tail contraction model [30]. In this experiment, the membrane of an amoeba is broken by taking an amoeba in a glass capillary, and then breaking the glass capillary. The cytoplasm was able to flow in multiple directions even without the contracting uroid suggesting that the tail contraction model is not the only mechanism for cytoplasmic streaming [31, 35]. Other experiments followed further showing that the pressure gradient was not the sole driving force behind amoeboid locomotion [30, 36, 37]. However, there is still no direct evidence showing either theory to be correct or incorrect, and thus the debate on the amoeboid motility mechanism continues.

Chapter 4

Models for the Whole Skin Locomotion Mechanism

Inspired by the cytoplasmic streaming motility mechanism of monopodial single cell organisms like the amoeba, we propose the WSL mechanism as an alternative locomotion strategy for mobile robots. Directly imitating the tail contraction model or the frontal-zone contraction model of the cytoplasmic streaming process is very difficult to do, if not impossible, since it would be very challenging to implement something similar to the endoplasm-ectoplasm transformation in macro scale (using electrorheological or magnetorheological fluids maybe some possible ideas for implementing this). Thus, instead of using the process of liquid-to-gel cytoplasm transformation, we plan to implement WSL using a flexible membrane skin (or a mesh of links) in the shape of a long torus. The skin of this elongated torus can then rotate in the longitudinal direction, turning itself inside out in a single continuous everting motion, effectively generating the overall motion of the cytoplasmic streaming ectoplasmic tube in amoebae (Figure 4).

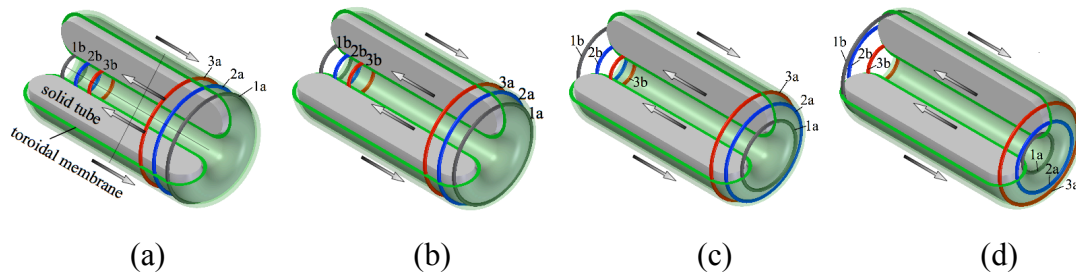


Figure 4. Motion generated by the rear contractile rings (1a, 2a, 3a) and frontal expansile rings (1b, 2b, 3b) for the concentric solid tube (CST) model.

The proposed WSL mechanism will have a structure of a toroid shaped skin, either with a solid tube inside (concentric solid tube model, CST), filled with liquid (fluid filled toroid model, FFT), or in the form of a novel tensegrity mechanism using two-fold closed-loop tape springs (statically balanced tensegrity model, SBT.) The motion of the torus-shaped skin will be generated by contracting and expanding the skin itself, or by the actuation rings embedded in the skin using several different mechanisms as presented in the following section.

4.1 Rear Contractile Rings with CST

One mechanism of generating the motion of the toroid shaped skin with the CST model is to use contractile rings embedded into the skin. These rings are like the toroidal microfilament band Actomyosin Contractile Ring, located equatorially in a cell reproducing through division, which acts as a purse-string suture separating the two daughter cells in the final stages of cytokinesis. As the rings located in the rear contract in sequence as shown in Figure 4, the tension in the rings translates to a force pulling the outer skin via surface tension to generate the forward motion.

As the contractile ring (1a) near the edge begins to contract, it pulls itself over the rounded edge of the CST, pulling the currently inactive rings behind it as shown in Figure 4 (a). When the following contractile ring (2a) approaches the rounded edge, it begins to contract, adding to the force generated by the contraction of the first ring, as shown in Figure 4 (b). This process continues as the first rings begin to pass completely inside the tube, as shown in Figure 4 (d). The active rings will continue to pull the inactive rings, allowing for continuous motion.

This mechanism is very similar to the tail contraction model for the monopodial cytoplasmic streaming amoeba; however, instead of the liquid to gel transition, the tension in the ring is converted to the actuating force through direct interaction with the surface of the CST inside the skin. Thus, the friction between the surface of the CST and the inside surface of the toroid skin will have a significant effect on the overall efficiency of the mechanism. The cross section shape of the rear end of the CST will play an important role in determining the force transmission characteristics as well.

4.2 Frontal Expansile Rings with CST

This actuation mechanism model works in the opposite way to the method involving rear contractile rings with a CST. As the actuating rings embedded in the inner-diameter skin near the front expand in sequence, they pull the skin located inward the torus out, generating the forward motion of the body (Figure 4). Since flexible members generally transfer force through tension only and not through compression, the expansile ring method may be less effective (more prone to buckling) than the contractile rings approach. Nevertheless, the expansion of the frontal rings

is still necessary to not constrain the overall motion of the skin, even if they are not used for generating the force for achieving motion. Note that the frontal expansile ring mechanism is not exactly analogous to the frontal-zone contraction theory for the monopodial cytoplasmic streaming amoeba.

4.3 Wave Contractile/Expansile Rings with CST

One potential problem of the two proposed methods used with the CST model presented above is that only a small portion of the actuators are being used at a given time. To increase the usage of the actuators and the overall effectiveness of the mechanism, both of these approaches can be utilized not only in the front and rear of the body, but all over the surface of the CST by forming the tube in a wave shape on the inner and outer surfaces, such as a sinusoidal or a saw tooth wave. This would allow all of the actuating rings to drive the skin simultaneously, taking advantage of the whole surface of the robot and improving the overall effectiveness of the mechanism.

4.4 Rear Skin Contraction with FFT

Instead of using the CST inside the toroidal skin, it could be filled with liquid, which would provide certain benefits. First, this will eliminate the friction caused at the interface between the skin and the solid tube, and second, it will allow the necessary compliance for the robot to squeeze between obstacles and morph into different length and diameter shapes. This is similar to a common child's toy that is often referred to as a "water worm" or a "water wiggler." With liquid filling the inside of the toroidal skin, the mechanism of generating the skin motion changes significantly from the proposed models using a CST. The actuating rings on the outside would compress the rear end, which would cause the liquid to flow forward, pushing out the inner skin in the front forward, generating the motion of the skin. This would be like squeezing toothpaste out of a tube, with the tube continuously reforming at the front. This approach is the closest to the tail contraction theory for the monopodial cytoplasmic streaming amoeba.

4.5 Actuation Methods and Packaging

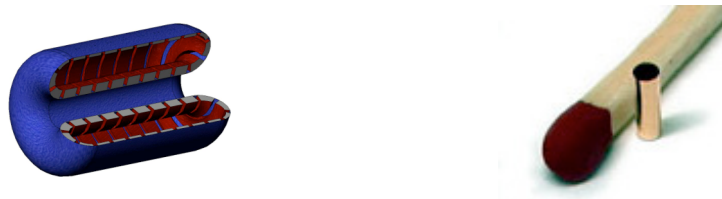
The WSL mechanism is a new class of mechanism that converts contracting and expanding motion of a ring to a toroidal everting motion. Thus, it does not require conventional actuators such as electric motors or linear actuators. To actuate the contracting and expanding rings to generate the desired motion for the WSL mechanism, two different methods are proposed, one method for the larger-scale implementation (Figure 5) and the other for the smaller-scale implementation (Figure 6).



(a) WSL with pressurized expandable hoses (b) Expanded (c) Contracted

Figure 5. Larger-scale actuation strategies.

The larger-scale method consists of rings of accordion-type hose that are expanded and contracted using pressurized fluid, such as compressed air, as shown in Figures 5 (b) and (c). The benefit of this strategy is that a large displacement (strain) can be obtained easily and the actuation force can be made large since it simply depends on the pressure of the fluid in the expanding hoses. These expanding rings can be embedded into the skin of the robot as channels, making it a robust approach for generating the rotating toroidal motion.



(a) WSL with electroactive polymer rings (b) An EAP tube with 1 mm diameter (Micromuscle AB)

Figure 6. Smaller-scale actuation strategies with EAP.

The smaller-scale method being considered uses rings of electroactive polymer (EAP) strips around the toroid to drive the motion (Figure 6). EAPs are active polymeric materials in which a stress and strain can be generated by the application of voltage and current (Figure 6(b)) [39]. Active materials may be the ideal actuators for WSL, since the strain they are able to produce is the type of displacement needed for WSL. Though promising, the general problem of this approach is the lack of force generated by these active materials [40]. Thus, EAPs are only considered for small-scale implementations. Among the many different types of EAPs, ionomeric polymers in particular will be studied for this application. Ionomeric polymers operate through the exchange of electrons and ions between a polymer and an electrolytic solution driven by an electric field between them. Thus ionomeric polymers must remain wet for the motion to take place, which is normally a problem for most applications [41]. However, this is not a concern for the FFT model as it needs to be filled with some kind of fluid.

The unique topology and nature of the everting motion of WSL presents practical challenges in packaging such as sensor integration, power delivery to the actuators and so forth. Since the entire outer skin rotates, attaching sensors to it becomes a problem. Moreover, packaging the power source and electronic components inside the robot becomes challenging. We have several ideas for addressing these issues, one of them shown in Figure 7. The cylinder located at the center of the robot with caps at both ends serves as the body for the robot which the skin everts around it. This cylinder, the “dog bone” as we call it, may house the power source and supporting components. The tapered end caps prevent the toroid skin from sliding off the cylinder and also provide the ideal location for mounting sensors such as cameras or others depending on the application. However, this work focuses on the study of actuation mechanisms for WSL. We hope this new paradigm in locomotion will inspire others to produce novel component technologies such as chemical power sources, membrane embedded micro-channels to connect the expanding and contracting hose actuator pairs, micro pumps, and other components which may be applicable to future implementations of robots that use WSL.

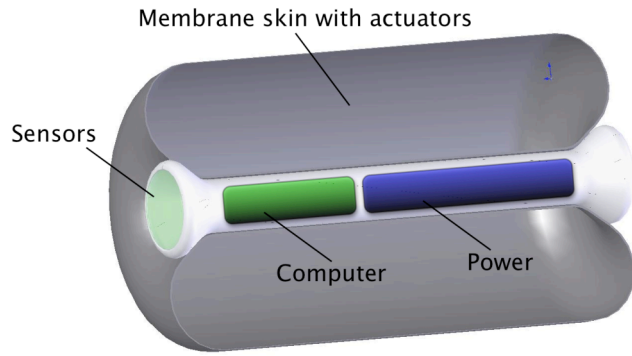


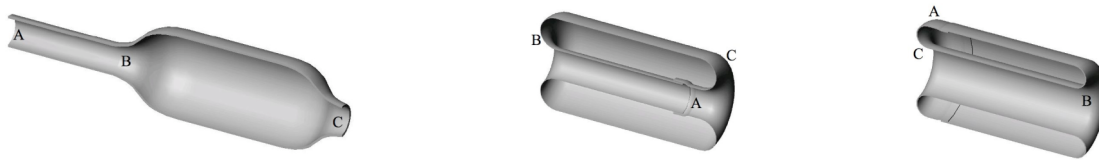
Figure 7. One possible example for component packaging; the “dog bone” concept.

Chapter 5

Feasibility Experiments

5.1 Feasibility Experiment with Pre-Tensioned Elastic Skin

A simple experiment was conducted using a long, elastic, silicone-skin toroid filled with water to demonstrate the feasibility of the WSL mechanism. The model is constructed with a tube of elastic silicone film with the diameter of half of the tube (section AB) smaller than the other side (section BC), as shown in Figure 8 (a). The two ends of the tube (A and C) are then pulled together, and the assembly is rolled into itself and sealed to form a long toroid shaped membrane. The membrane is then filled with water at a pressure typical of a water balloon (Figure 8 (b)).



(a) Construction (b) State of low potential energy (c) State of high potential energy

Figure 8. Construction of a pre-tensioned elastic skin FFT model and its energy states.

When the tubular section of the smaller diameter (section AB) is rolled into the center, and the section of the larger diameter (section BC) is rolled outward to form the outer skin, the model assumes the lowest energy state as shown in Figure 8 (b). However, when the entire skin is rotated and flipped “inside out” such that the section of the larger diameter (section BC) is rolled into the center, and the tubular section of the smaller diameter (section AB) is rolled outward, the outer elastic skin is now stretched, assuming the high potential energy state as shown in Figure 8 (c). Starting from this position with a slight bias to direct the motion to the right (Figure 9 (a)), the skin of the FFT rotates to reach its lowest energy state (Figure 9 (c)) moving the toroid to the right like a three-dimensional tread.

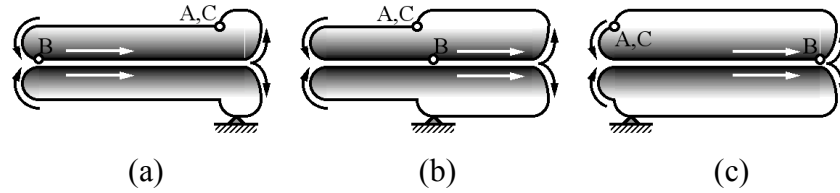


Figure 9. Motion of the pre-tensioned elastic-skin FFT model.

The mass of the FFT model used for the experiment is 0.369 kg with a length of 25 cm and a nominal outer diameter of 5 cm. A sequence of pictures of the actual motion of this pre-tensioned skin model is shown in Figure 10. The model traveled the distance of its full length of 25 cm in 0.46 seconds (average 0.54 m/s). This simple demonstration shows the feasibility of the WSL mechanism. With a continuous contractile actuation of the outer skin in the rear, the toroid will be able to continuously move in the forward direction.

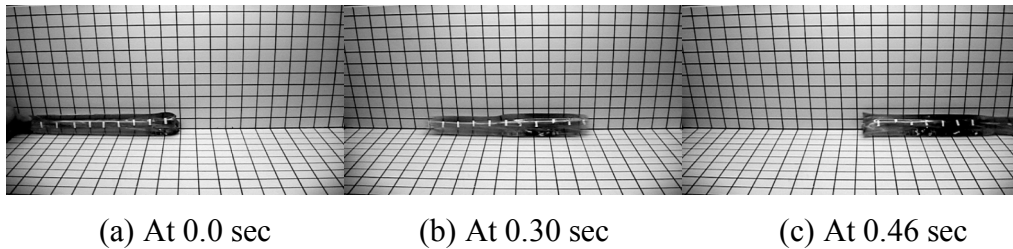


Figure 10. Sequence of pictures of the locomotion of the pre-tensioned elastic-skin model.

5.2 Rear Skin Contraction Experiment Using Tension Cords

Another simple experiment was conducted to demonstrate the feasibility of generating the forward motion by active contractile actuation of the outer skin. The apparatus used in this experiment was a jig (Figure 11) with a number of tension cords wrapped around the FFT such that when the cords are pulled, the loops will contract the outer skin to generate the necessary tension to produce the everting motion. By pulling the cords in sequence to contract the outer skin, the FFT moved forward (Figure 11).

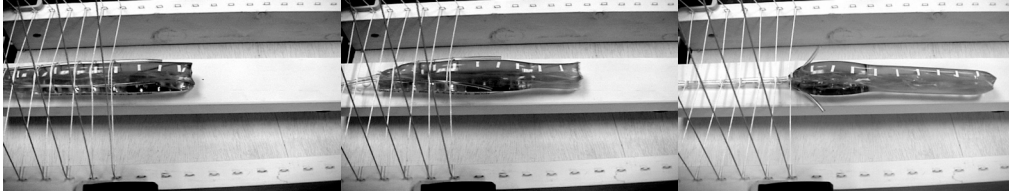


Figure 11. Sequence of pictures of the tension cord actuated model locomotion.

When all the cords are pulled in the same amount at once, the overall diameter of the toroid decreased while the overall length increased since the fluid inside the body is incompressible. This transformation into different diameters and lengths could be useful for the robot to morph into different shapes. The effect of the sequence of pulling the cords to the motion and shape change of the body will be further investigated.

Chapter 6

Analysis of the CST Model

Nomenclature

η	Efficiency of a single actuating ring over a CST
μ	The coefficient of Coulomb friction between the contracting ring and the CST surface
ϕ	The slope angle of the CST surface in the longitudinal direction
c	The circumference of a contracting ring actuator [length]
f	Distributed force along the inside of a contracting ring in the radial direction (the “squeezing” force of an actuator ring on the CST surface) [force/length]
f_f	Distributed friction force in the longitudinal direction between the contracting ring and the CST surface [force/length]
f_N	Distributed normal force on the surface of a CST in the radial direction due to a contracting ring actuator [force/length]
f_R	Distributed output “propulsion” force in the longitudinal direction of a single contracting ring actuator [force/length]
$f_{T,l,m}$	Distributed tension force on a skin segment between two actuating rings, acting from ring l to ring m [force/length]
F	The total propulsion output force generated by a contracting actuation ring(s) [force]
MA	Mechanical advantage, defined as the output force divided by the input force
R	The radius of a contracting ring actuator [length]
s	Position of an actuation ring represented as the distance from a fixed reference on the CST, along its travel path on the CST surface in the longitudinal direction [length]
T_R	Tension in a contracting ring actuator [force]
n	The nominal number of actuating rings per unit length in the longitudinal direction assuming equal distribution
N	The number of active contracting actuator rings
x	Horizontal position coordinate of the actuator ring
y	Vertical position coordinate of the actuator ring

6.1 Mechanics of a Single Actuation Ring Over a CST

The WSL CST model is driven using a series of expanding and contracting rings over a solid core. A simplified quasi-static force analysis was performed on the CST type body with rear contractile rings first to gain insight into the mechanics of the simplest WSL mechanism actuation model. Figure 12 shows the free body diagram of a single contracting ring at the instant when its radius is R and when it is squeezing the skin over the CST with a distributed force of f (unit: [force]/[length]).

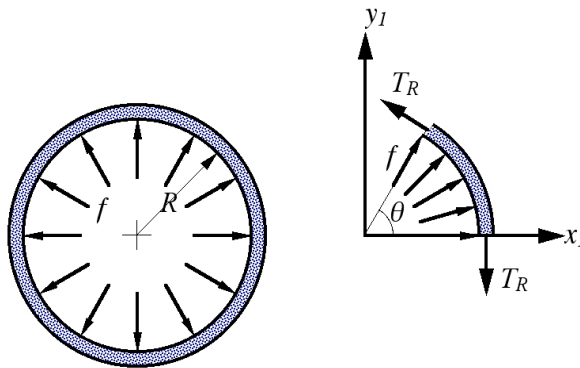


Figure 12. Free body diagram of a contracting ring actuator.

The relationship between the tangential direction tension in the contracting actuator T_R , and the distributed “squeezing” force f in the radial direction can be found by integrating f over a segment of angle θ , and summing the forces:

$$\sum F_{x1} = 0 \rightarrow \int_0^\theta f \cos \theta \cdot R \cdot d\theta - T_R \sin \theta = 0 \rightarrow f = \frac{T_R}{R} \quad (1)$$

where the contracting distributed force f is inversely proportional to the actuating ring radius R , and proportional to the tension (T_R) it can generate. For the expanding rings, the relationship is similar to this where the expanding ring distributed force f on the outside is also inversely proportional to the actuating ring radius R , and proportional to the compression it can generate.

From the mechanics of the interaction with the actuator rings, a CST with the simplest cross-section geometry (straight lines with round edges) can be divided into four different active regions and two passive regions. The two passive regions are the outside and the inside straight line surfaces of the CST, and the four active regions shown in Figure 13. The first active region

(region I) is where the ring contracts over the outer curved surface of the CST, the second active region (region II) is where the ring contracts over the inner curved surface of the CST. The third active region (region III) is where the ring expands over the inner curved surface of the CST, and the fourth active region (region IV) is where the ring expands until it reaches the outer passive region.

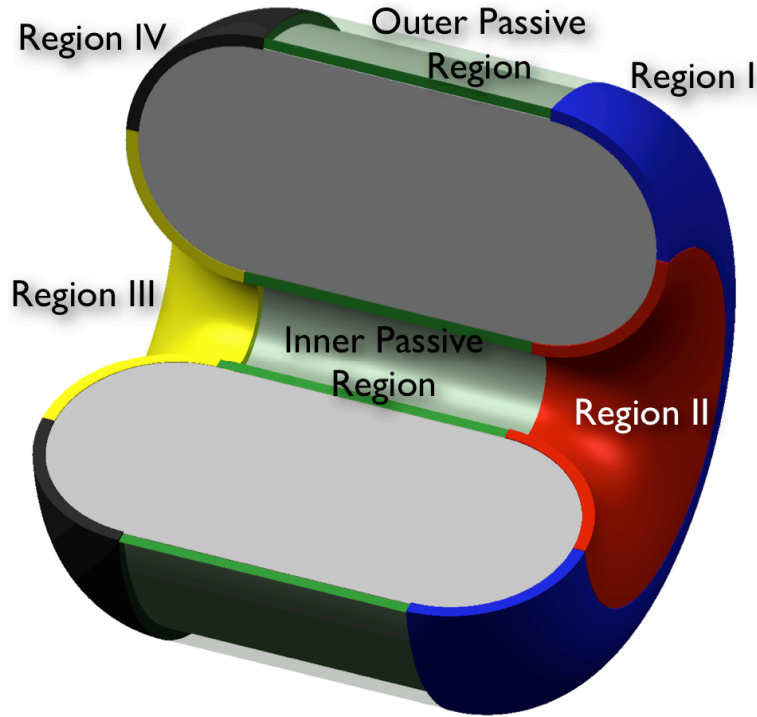


Figure 13. The four active and two passive regions of the straight line with round edge CST.

Mechanics of CSTs with other geometries can be analyzed using these basic 4 active region types. For example, the wave contractile/expansile rings with CST model using the sinusoidal wave shape tube on the inner and outer surfaces can be analyzed with a combination of many of these 4 types of active regions all over its surface. The mechanics of the actuating rings in these four regions are investigated in the following next four sub-sections.

6.1.1 Region I

Region I is the active region of most interest, because active materials that can be used for this application such as EAPs and SMAs (the most likely actuator materials) primarily act in

tension. Also, as will be explored in the following sub sections, actuation in other active regions (regions III and IV) by expansion of the actuator rings can experience problems with buckling.

Assuming Coulomb friction between region I of the CST and the inner surface of the membrane, with a friction coefficient μ , the free body diagram for a segment of the membrane between region I of the CST and the single contractile actuation ring is shown in Figure 14.

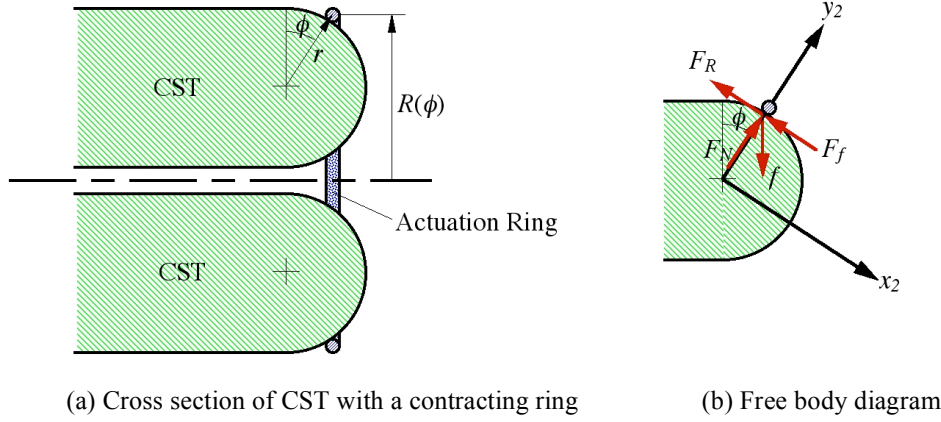


Figure 14. Free body diagram of a membrane segment between the contractile ring and region I of the CST.

A quasi-static force balance shows the relationship between the contracting distributed force (and through Equation 1, the tension T_R) in the actuator, and the distributed output “propulsion” force f_R in the longitudinal direction (unit: [force]/[length]) a single contracting ring can generate as a function of the slope angle $\phi(x)$ of the CST at the location and the ring radius $R(x)$.

$$\begin{aligned}
 \sum F_{y2} = 0 &\rightarrow f_N = f \cos \phi(x) \\
 \sum F_{x2} = 0 &\rightarrow f_R + f_f = f \sin \phi(x) \rightarrow f_R = f(\sin \phi(x) - \mu \cos \phi(x)) \quad (2) \\
 \rightarrow f_R &= \frac{T_R}{R(x)} (\sin \phi(x) - \mu \cos \phi(x))
 \end{aligned}$$

The radius of the actuating ring $R(x)$ is a function of the position (x) of the actuation ring over the CST and will also depend on the longitudinal cross-section geometry of the CST (shown as semicircular in Figure 14).

The total output “propulsion” force of a single contracting ring over a CST is found by multiplying the longitudinal output force per unit tangential length (f_R) by the circumferential length over which it acts ($2\pi R(x)$). This leads to the following input-output relationship:

$$F(x) = T_R 2\pi(\sin \phi(x) - \mu \cos \phi(x)) \quad (3)$$

From this it can be seen that the total output “propulsion” force F of a single contracting ring over a CST is only dependent on the friction coefficient and the slope angle $\phi(x)$ of the CST at the location of the actuating ring, thus the friction and end shape of the CST will have a great effect on the force transmission characteristics and the efficiency of the mechanism, as will be shown in the following sections.

6.1.2 Region II

The second active region of the CST is the inner part of the rear of the body, as shown in Figures 13 and 15. The way in which the propulsive force is generated by the actuating rings in this region is very different from that of region I, as there is no direct interaction between the surface of the CST and the membrane or the actuating rings. Rings in this region contract and pull the membrane skin inward, generating the propulsive force even though they are not able to directly push off the surface of the CST.

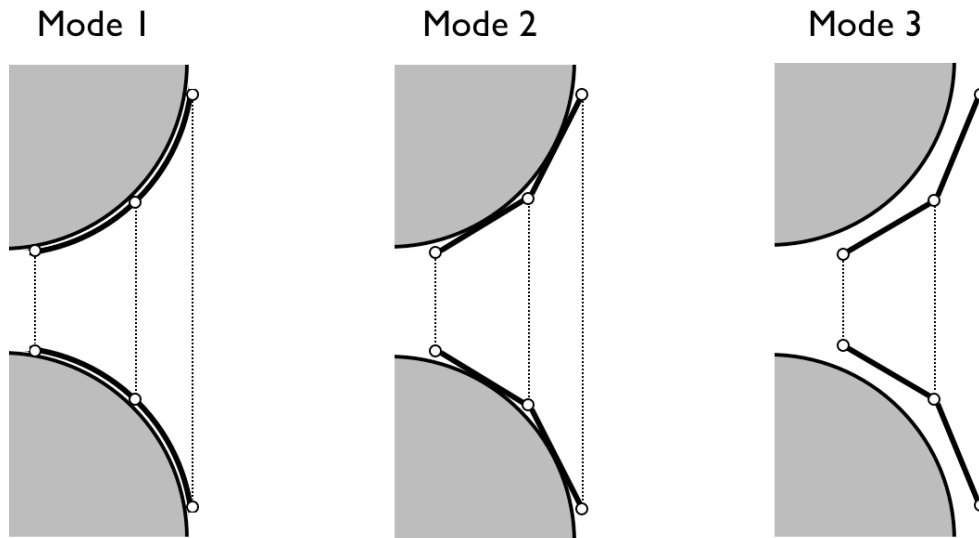


Figure 15. The three modes of operation in region II, fully in contact (mode 1), partially in contact (mode 2), and no contact (mode 3).

There are three modes of operation in this region, depending on the contact state of the rings and membrane skin to the CST surface as shown in Figure 15. The rings and the skin can both be fully in contact with the surface of the CST (Figure 15-a), the rings can be out of contact with the body while the connecting skin segments are in contact with the surface of the CST (Figure 15-b), or both the rings and connecting skin segments can be out of contact with the surface of the CST (Figure 15-c), depending on the state of actuation. In this last mode of operation there will be no friction between the membrane skin and the surface of the CST thus it may be the most desirable way of operating.

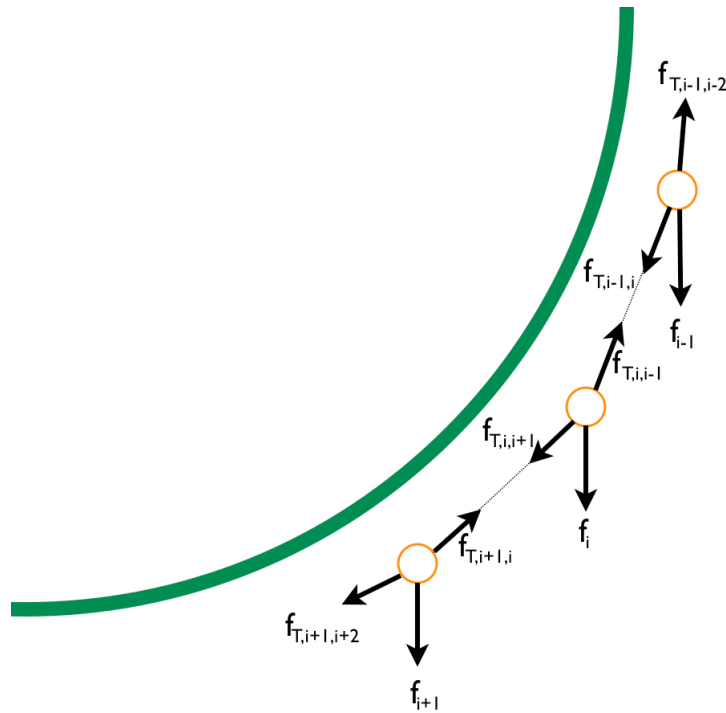


Figure 16. Free body diagram of multiple actuating rings in Region II.

The free body diagram of actuating rings in the last mode of operation is shown in Figure 16. From this it can be seen that each ring is a three-force member, with one force from the distributed squeezing force of the ring (f_i), and with one each from the tension in the membrane skin attached before ($f_{T,i,i-1}$) and after ($f_{T,i,i+1}$) the ring. Figure 17 shows the force vector polygon for this three force member. From the law of sines the following relationship between the three forces can be found:

$$\frac{f_i}{\sin \gamma_i} = \frac{f_{T,i,i-1}}{\sin \beta_i} = \frac{f_{T,i,i+1}}{\sin \alpha_i} \quad (4)$$

where f_i is the distributed squeezing force of ring i , $f_{T,i,i-1}$ is the distributed tension force from ring i to ring $i-1$, $f_{T,i,i+1}$ is the distributed tension force from ring i to ring $i+1$, and α_i , β_i and γ_i are the angles between the force vectors as shown in Figure 17.

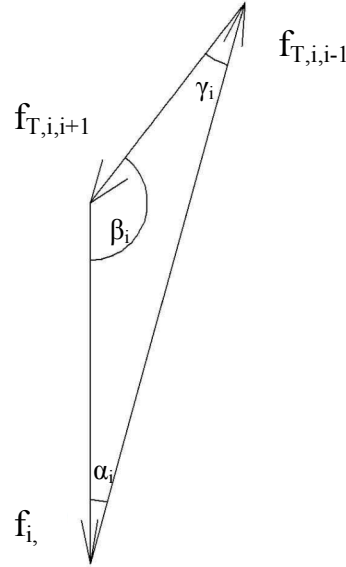


Figure 17. The actuation ring in Region II as a three-force member.

If the connecting segments are not in contact with the body, as shown in Figure 16, these angles can be calculated using the coordinates of the three actuation rings.

$$\begin{aligned} \alpha_i &= \tan^{-1} \left(\frac{x_{i-1} - x_i}{R_{i-1} - R_i} \right) \\ \beta_i &= 180^\circ - \tan^{-1} \left(\frac{x_i - x_{i+1}}{R_i - R_{i+1}} \right) \\ \gamma_i &= 180^\circ - \alpha_i - \beta_i \end{aligned} \quad (5)$$

where x and R are the coordinates of ring i , the leading ring (ring $i+1$) and the following ring (ring $i-1$). If the segments are in contact with the body, as with modes 1 and 2 in Figure 15, then the angles will depend on both the amount of the segments in contact with the CST, and the

material properties of the segments and ring actuators. Therefore, the angles will have to be redefined for mode 1 and 2, based on and their individual characteristics.

The position and output of a single ring will be determined not only by its position and squeezing force, but also by the position and squeezing force of the next and previous rings as well. The output force of a ring in region II will be the difference of the tension between the two connecting segments attached to it. Thus, using Equation 4, the following equation can be derived:

$$f_{R,i} = f_i \frac{\sin \beta_i}{\sin \gamma_i} - f_{i-1} \frac{\sin \alpha_{i-1}}{\sin \gamma_{i-1}} \quad (6)$$

To convert this distributed output force to force output of the pair of rings, it must be multiplied by the average circumference of those rings (as shown in Equations 2 and 3).

If the rings are constrained to move along a circular profile α , β and γ can be put in terms of the slope angle of the actuating rings:

$$\begin{aligned} \alpha_i &= \phi_i - \frac{\Delta\phi}{2} \\ \beta_i &= \pi - \phi_i - \frac{\Delta\phi}{2} \\ \gamma_i &= \Delta\phi \end{aligned} \quad (7)$$

where ϕ_i is the slope angle of ring i , and $\Delta\phi$ is the difference in slope angle between the rings. Using this, and Equations 1 and 6, the force output of a pair of rings can be determined in terms of the slope angle:

$$F_i = \pi(2R_{\max} - r \sin \phi_i - r \sin(\phi_i - \Delta\phi)) \cdot \frac{\frac{T_{R,i}}{R_{\max} - r \sin \phi_i} \sin\left(\phi_i + \frac{\Delta\phi}{2}\right) - \frac{T_{R,i-1}}{R_{\max} - r \sin(\phi_i - \Delta\phi)} \sin\left(\phi_i - \frac{3 \cdot \Delta\phi}{2}\right)}{\sin \Delta\phi} \quad (8)$$

where R_{\max} is radius of a ring at the tip of the CST, and r is the radius of the circle the rings are constrained to travel over. From this it can be seen that the mechanics in region II is much more complex, and dependent on more variables than that in region I. Here the output force is dependent on spacing of the rings, the difference in ring tension, and dimensions of the CST, not just the slope angle itself.

6.1.3 Region III

Region III is the area of the CST where an expanding ring pushes against the front, inner surface. This front expanding ring will generate the propulsive force in a similar way as the rings in Region I, but by pushing off the CST surface by the expansion of the ring.

It is important to note that since the actuator rings in this region are expanding, they will no longer be under tension, but under compression. Flexible actuators, such as ones that use electroactive polymers or shape memory alloys, may cause problems in buckling when put under compression. While the rings still need to expand in order to prevent interference with the motion over the body of the CST, it is unlikely that they will provide useful work to the system. In some cases the actuators may also contract slightly from its nominal diameter to hold the membrane skin and rings away from the surface of the CST to reduce friction. This may be done if the energy loss from the friction is greater than the energy required to hold them away.

6.1.4 Region IV

The final active region is Region IV, the frontal expansion region. Similar to the relationship between Region I and Region III, the mechanics of this region behave as the inverse of Region II. The same caveats on actuating in Region III also apply to this region. While a ring in Region IV could potentially provide useful work input, it would also be operating in compression thus, as in Region III, there is the potential problem of buckling. Nevertheless, the actuating rings need to expand enough to prevent interference of motion over the CST surface.

6.2 Mechanical Advantage and Efficiency for Different Cross-section geometries

As was shown in Sub-section 6.1.1 the output of a ring contracting or expanding against a CST is dependent on friction and cross-section geometry. The mechanical advantage and efficiency can be used to observe the force transmission characteristics and energy loss of the mechanism over its range of motion. In this section we define mechanical advantage and efficiency for a WSL mechanism with a CST, and present a parametric study of how various parameters such as position, friction coefficient, and CST cross-section geometry affect the total output force and the total output work for a CST WSL mechanism.

The mechanical advantage is used to observe how the total force output of the mechanism changes over the ring actuator's range of motion, for a given ring actuator contracting force. For

this system the mechanical advantage is defined as the ratio of the total propulsion output force F over the actuating ring tension input force T_R .

$$M.A. = \frac{F}{T_R} \quad (9)$$

Similarly, the efficiency of the system is defined as the ratio of the output work over the input work by the actuation ring.

$$\eta = \frac{W_{out}}{W_{in}} = \frac{F \cdot \Delta s}{T_R \cdot \Delta c} \quad (10)$$

where Δs is the distance the actuation ring travels on its path, and Δc is the change in the circumference of the actuation ring. The efficiency of the mechanism will show how much work is lost through the friction between the ring actuator and the CST surface.

6.2.1 Round Cross-section, Region I

In this section we observe how changing the Coulomb friction coefficient between the actuation ring and the CST affects the mechanical advantage and efficiency in region I of the WSL mechanism with a round cross-section over its range of motion. Figure 18 shows the efficiency and mechanical advantage of a WSL mechanism with a single actuation ring in region I on a semi-circular cross-section CST body (as shown in Figure 14) plotted against its travel path length with varying friction coefficients (from 0.01 to 1.0).

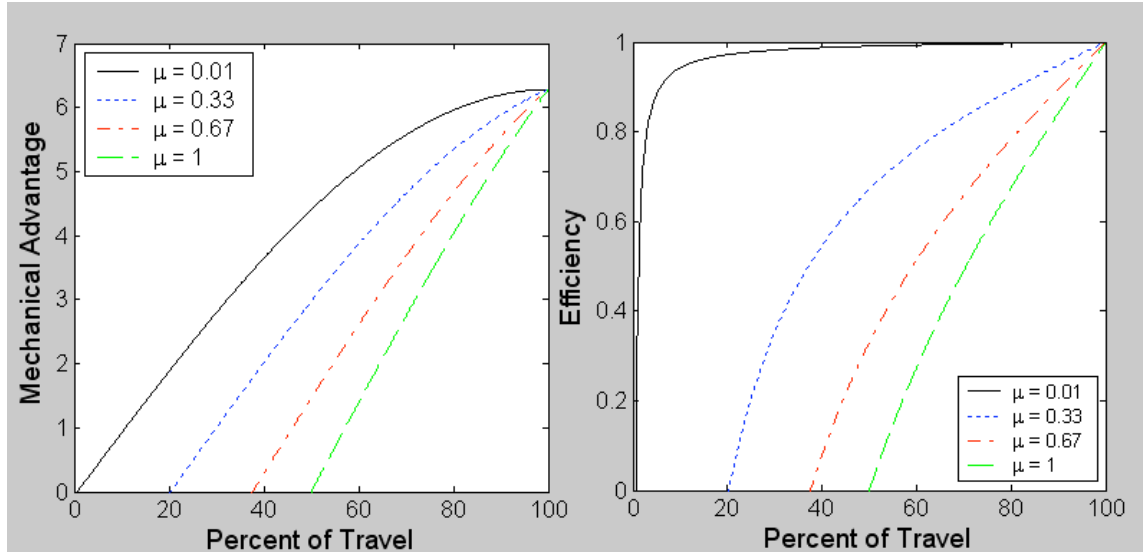


Figure 18. Mechanical advantage and efficiency versus percent of travel for a circular cross-section CST in Region I with varying friction coefficients.

For the case of a semi-circular cross-section CST, both mechanical advantage and efficiency show similar trends of becoming larger as the contracting ring moves from its initial position with values of zero, to its final position where they reach their maximum values. The mechanical advantage and efficiency for a given friction coefficient is simply a function of the slope angle ϕ and when the CST is flat, perpendicular to the radial direction of the contracting ring, all of the “squeezing” force, f , is used against the normal force, f_N , producing no output force. When the contracting ring reaches the tip of the CST (the end of region I and beginning of region II), the “squeezing” force of the ring actuator is in the contact tangential direction, thus there is no friction loss and all of the input force is transferred into the total output force, resulting in an efficiency of 1. At this position, the mechanical advantage also reaches its maximum value of 2π , which is the ratio between the circumference (tangential direction) and the radius (radial direction) of the circular cross section of the CST. This maximum value is the same for all friction coefficients as there are no contributions from friction at this position.

The friction coefficient has a large effect on both the mechanical advantage and efficiency of the mechanism, as can be seen in Figure 18. The lower the friction coefficient is the faster the efficiency approaches the maximum value, and the sooner it can produce useful work. From these two figures we can observe that a single contracting ring actuator cannot produce any useful work until it reaches a certain critical point (where the curve intersects the x-axis.) This is

the point where the propulsion force from the tension in the ring actuator can start to overcome the friction force resulting from the normal component of the squeezing force. The location of this critical point varies from the beginning of the range of motion, for a very small friction coefficient, to half way along the active surface of the cross section, for the maximum coefficient of 1, as this is where the slope angle ϕ equals the inverse tangent of the friction coefficient.

From these observations, the optimal actuation strategy for the many actuation rings (how much tension in each actuation ring in which sequence) can be developed to maximize the output work. Also, in the design phase, insights obtained from this can be applied in deciding the distribution of the actuating rings in the membrane skin to ensure smooth motion of the mechanism, and minimize the number of actuators.

6.2.2 Straight Line Cross-section, Region I

For a straight line (or triangular) cross-section CST geometry the friction and the slope angle ϕ are the only variables that influence the efficiency and mechanical advantage, as with the round cross-section CST geometry as shown earlier. However, unlike the circular cross-section case, a straight line cross-section has a constant slope; therefore, the mechanical advantage and efficiency are constant for a given slope and friction coefficient, as can be seen in Figures 19 and 20. Figure 19 shows the mechanical advantage and efficiency for various friction coefficients. In these plots the slope angle ϕ is held constant at 45° . Figure 20 shows the mechanical advantage and efficiency for various slope angles. These plots are shown without friction. From Figure 20 it can be seen that the most efficient cross-section is one with a slope angle of 90° , a vertical drop. This is the expected result, as when the slope angle is 90° all of the applied force is used for actuation.

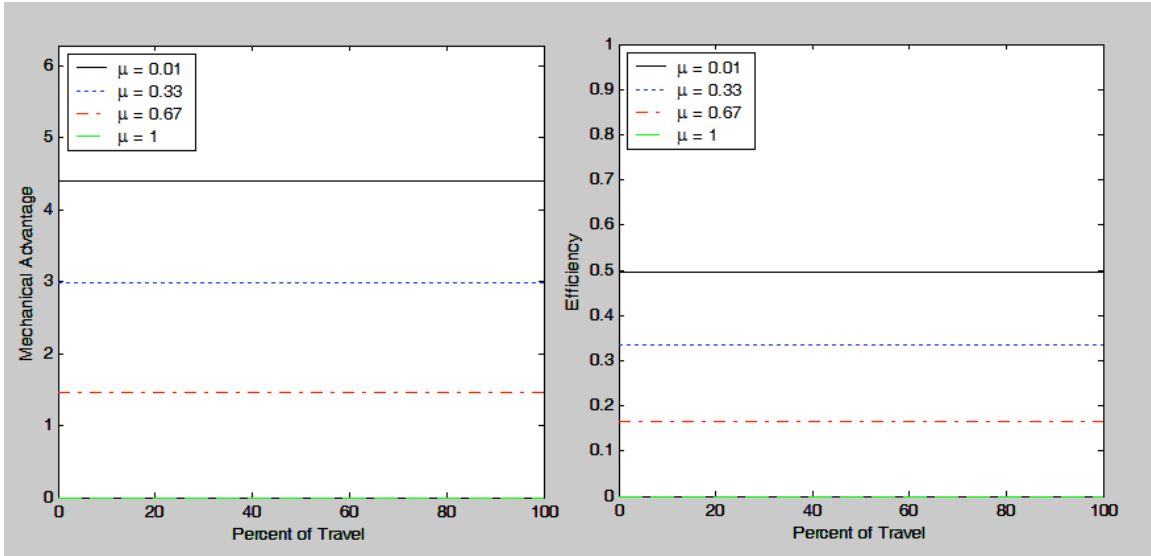


Figure 19. Mechanical advantage and efficiency of a strait line cross-section CST, for varying friction and a constant slope angle of 45° .

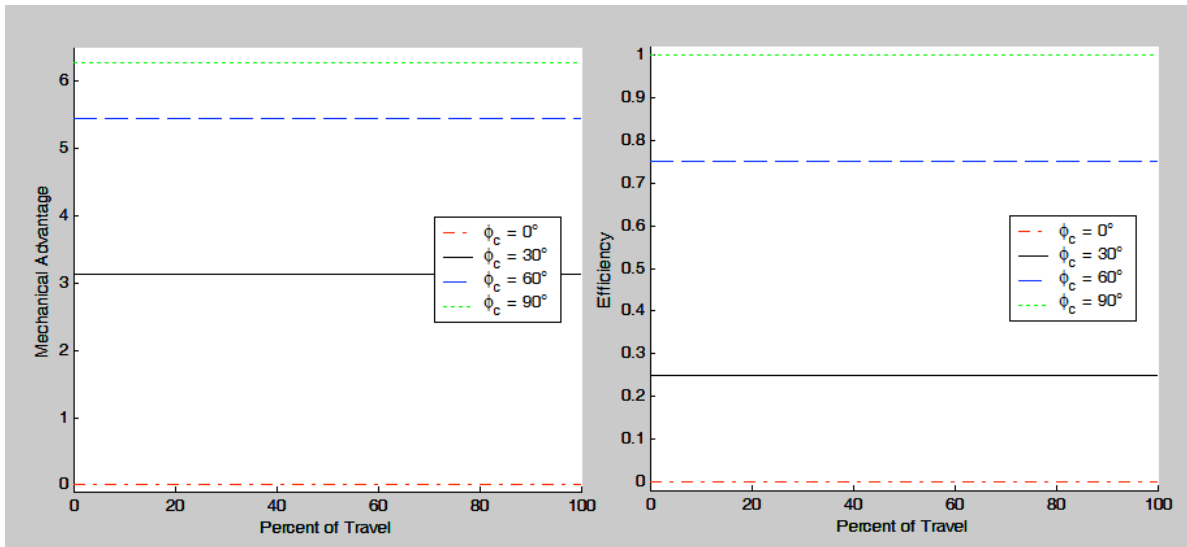


Figure 20. Mechanical advantage and efficiency of a strait line cross-section CST, for varying slope angles and a friction coefficient of 0.

With a straight line cross-section there will be two points where Region I starts and ends. At these points there may be a need for a rounded region of the cross-section for a smooth motion of the membrane skin moving over the surface of the CST. Also, depending on the output characteristics of the selected actuators, it may be preferable to have a mixture of cross-section geometries, with high and low mechanical advantage. Thus for an efficient cross-section geometry for a CST, a combination of strait line and round cross-sections may be preferable.

6.2.3 Composite Cross-section, Region I

In the previous subsections, a CST with a semicircular cross-section and a straight line cross-section were analyzed to see how various parameters affect the efficiency of the mechanism. As the efficiency and mechanical advantage depend on the slop angle at the location of the actuation ring, among other parameters, a CST with a combination of cross-sections can be utilized to increase the area of active region and to maximize the overall performance of the mechanism.

Analysis of a composite cross-sectional geometry is presented to observe how the changing of cross-section geometry changes the mechanical advantage and efficiency of the WSL mechanism over its range of motion along with the effect of the friction coefficient. The composite cross-sectional geometry of interest consists of a straight-line cross-section (or conical section: the segment of the cross section with a constant slope) with length l_2 , and two semicircular cross-sections (with radii r_1 and r_3) with a continuous transition between them, as shown in Figure 21.

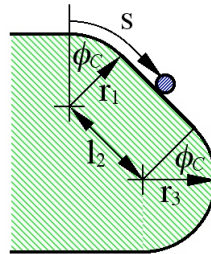


Figure 21. Composite cross-section CST.

Figure 22 shows the mechanical advantage and efficiency of this composite cross-section CST for various friction coefficients. In this model the angle of the area of constant slope is 45° and the parameters for r_1 , l_2 , and r_3 are all unit length. The plots for efficiency and mechanical advantage show similar trends in the two rounded cross section regions to the plots for the circular cross-section, shown in Figure 18. For the constant sloped cross-section region, the mechanical advantage and the efficiency are constant, the same as shown in the previous subsection. These plots also show that the critical point where the useful work can be produced occurs earlier than with a semicircular cross-section, for a given friction coefficient under 1. Thus by combining a strait cross-section with a round cross-section, we can increase the overall

efficiency and mechanical advantage and also increase the area of the active region (the region where the actuating ring can produce output force).

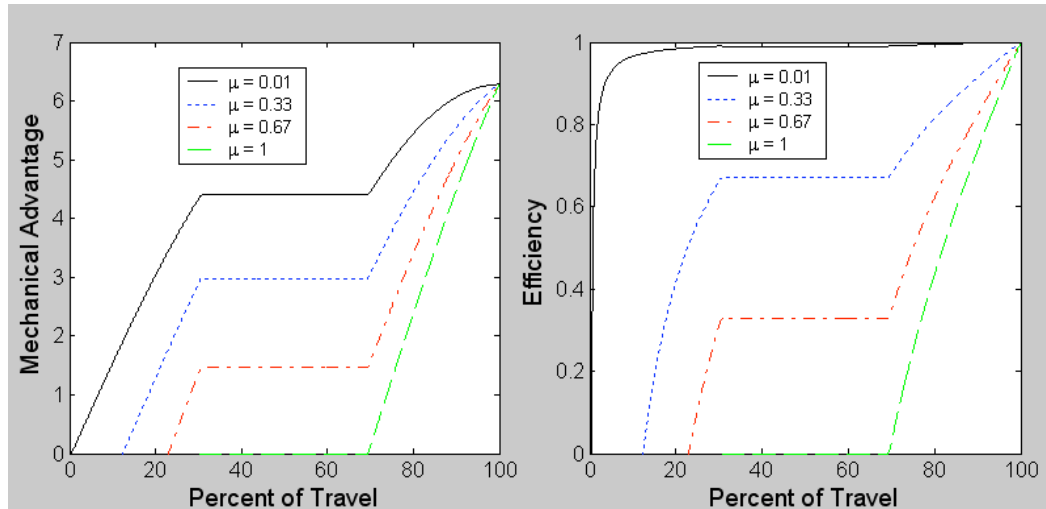


Figure 22. Mechanical advantage and efficiency for a composite cross-section CST with varying friction coefficients.

For this simple composite cross sectional geometry there are four geometric variables, the lengths of r_1 , l_2 and r_3 , and the angle of the area of constant slope, ϕ_C . For this analysis we want to observe how each of these variables affects the output.

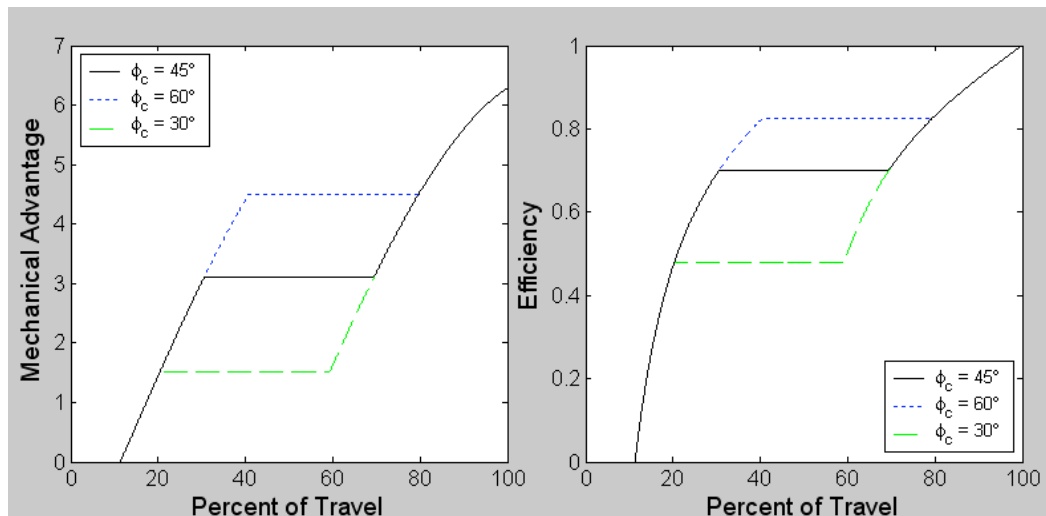


Figure 23. Mechanical advantage and efficiency for a composite cross-section CST with varying slope angles.

Figure 23 shows how changing the slope angle changes the shape of the mechanical advantage and efficiency plots. In this model the slope angle is varied from 30° to 60° , while the friction coefficient is kept constant at 0.3 and the parameters for r_1 , l_2 , and r_3 are all kept constant at unit length. Changing the angle of the area of constant slope of the middle section of the CST moves the constant mechanical advantage and efficiency region up or down, as was seen in the previous sub-section. Thus for systems with a high friction coefficient a more effective system could be constructed by increasing the slope of the middle section of the CST which could greatly increase the overall efficiency of the system.

Figure 24 shows how the other geometric parameters (r_1 , l_2 and r_3) change the shape of the mechanical advantage and efficiency plots. In this example, the angle of the area of constant slope and the friction coefficient are held at 45° and 0.3 respectively. The actual distance traveled rather than the percent of distance traveled is used in this plot, as changing the lengths changes the end points relative to each other.

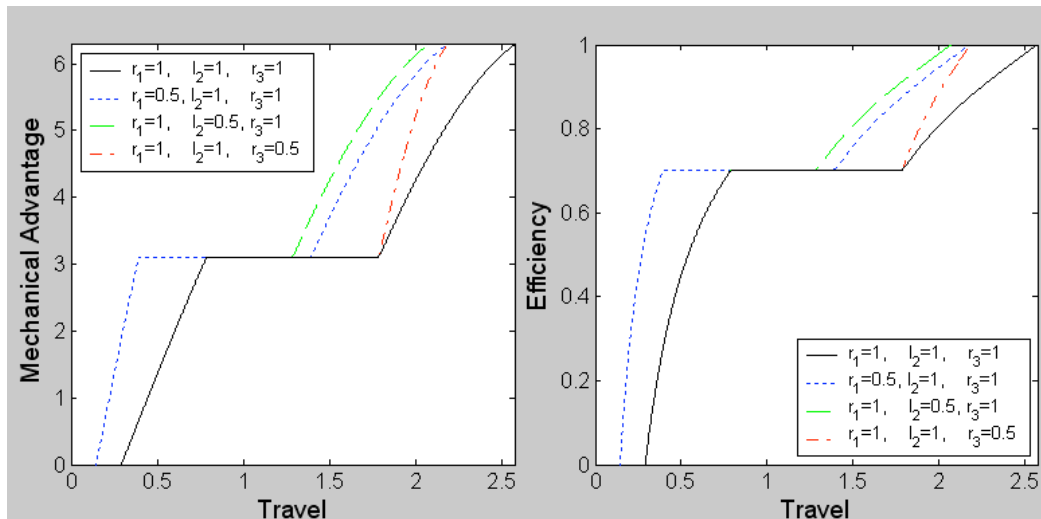


Figure 24. Mechanical advantage and efficiency for a composite cross-section CST with varying geometry.

From these plots it can be seen that if the radius of either the first or third section (r_1 or r_3) is shortened the slope of that section of the plot increases, and it will reach a higher mechanical advantage and efficiency sooner. Shortening the length of the second section (l_2) only changes the total distance traveled, and has no effect on the overall efficiency or mechanical

advantage. Again, this information will be useful in designing future CST WSL mechanisms to maximize the performance of the system.

6.2.4 Region II

As the force output for region II is based on the difference in tension between the actuating rings connected by a membrane segment, the mechanical advantage of rings in region II is calculated using F_i from Equation 8, and dividing by the average of the input forces of the two actuating rings:

$$MA_i = \frac{F_i}{(T_{R,i} + T_{R,i-1})/2} \quad (11)$$

Expanding this equation in terms of Equations 1, 7 and 8 results in the following equation:

$$MA_i = \frac{\pi(2R_{\max} - r \sin \phi_i - r \sin(\phi_i - \Delta\phi))}{\sin \Delta\phi} \left(\frac{\sin\left(\phi_i - \frac{\Delta\phi}{2}\right)}{R_{\max} - r \sin \phi_i} - \frac{\sin\left(\phi_i - \frac{3 \cdot \Delta\phi}{2}\right)}{R_{\max} - r \sin(\phi_i - \Delta\phi)} \right) \quad (12)$$

Figure 25 shows the mechanical advantage of a round cross-section CST in region II, with a constant ring tension (T_R). In this plot the rings move along a circle with a radius of unit length, the radius of the inside of the CST (the minimum ring radius) is unit length, and the angle between the rings varies from 1° to 30° .

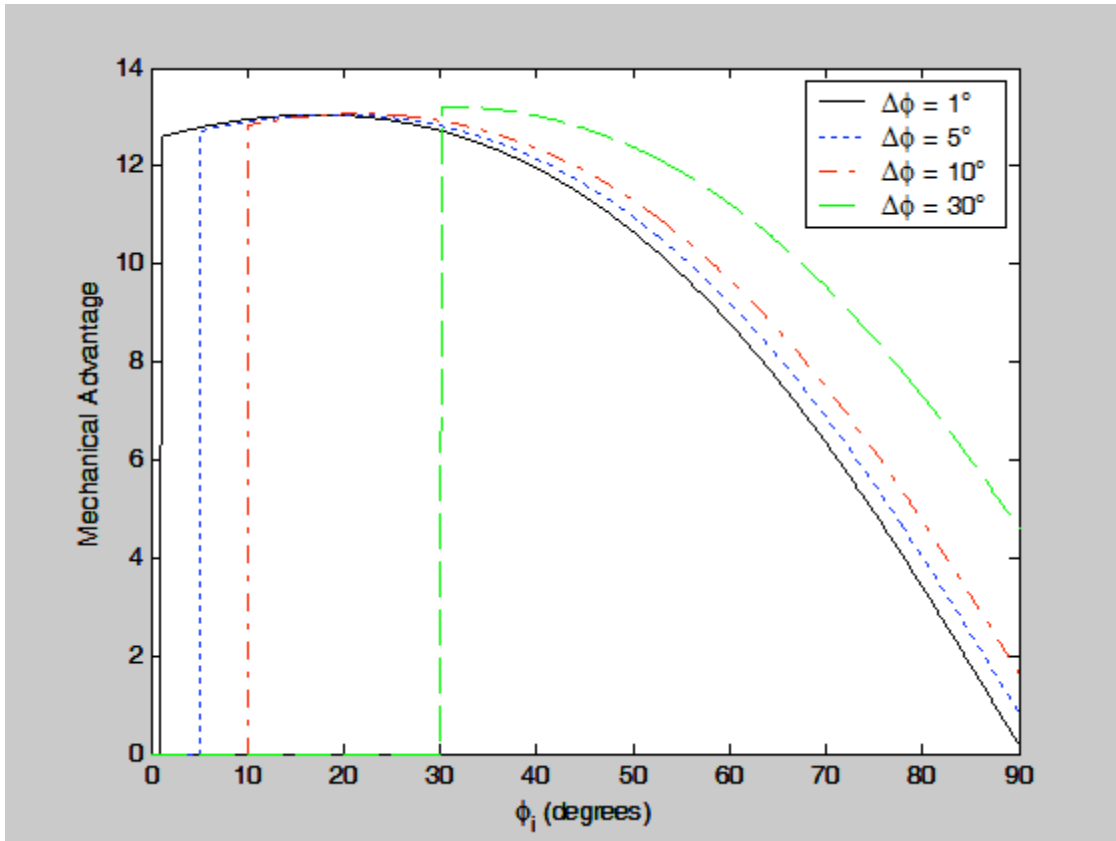


Figure 25. Mechanical advantage of the round cross-section, region II, mode 3, with unit ring tensions, and varying ring spacing.

In this plot, instead of using the percent travel, mechanical advantage is plotted with respect to the slope angle of ring i , and each plot begins when ring $i-1$ leaves region I. As with region I, the maximum mechanical advantage occurs when the ring is closest to the tip, and the minimum occurs when the ring is closest to the inside of the body. From this plot it can be seen that as the spacing between the rings increases, the overall mechanical advantage increases. This is because the larger ring spacing increases the angle between the rings, which increases the difference in tension between rings i and $i-1$.

As with modes 1 and 2 (shown in Figure 15), Equations 4-8 are only valid if the ring of interest is a three force member. Therefore, we can only look at the round cross-section, as the forces for triangular or composite cross-sections will include a straight section, and will not form a valid force triangle. If a valid force triangle is not formed, the forces in the segment will be statically indeterminate, meaning that we would have to look at specifics of materials and actuators, which is beyond the scope of this research.

6.2.5 Region III and IV

Regions III and IV, the front expanding ring area, will have the same mechanical advantage and efficiency behavior as the rings in Regions I and II respectively. Again, it is important to note that since the actuator rings in this region are expanding, they will no longer be under tension, but under compression. Flexible actuators, such as ones that use electroactive polymers or shape memory alloys, could be problematic as they could buckle while under compression. The rings still need to expand in order to prevent interference with the motion over the body of the CST; however, it is unlikely that they will provide useful work to the system.

6.3 Analysis and Simulation for the CST Model System

6.3.1 Displacement Constraints of the Actuation Rings for the CST Model System

As each ring moves across the surface of the CST it will need to follow a set pattern. The pattern for a circular cross-section is shown in Figure 26. The ring starts on the outer surface of the CST, contracts over Region I ($x = 0$ to 0.5) and contracts inside Region II ($x = 0.5$ to 1.0), then passes through the inner surface of the CST ($x = 1.0$ to 2.0). It then expands inside Region III ($x = 2.0$ to 2.5), expands over region four ($x = 2.5$ to 3.0), and returns, through Region IV ($x = 3.0$ to 4.0), to the beginning of Region I ($x = 0$).

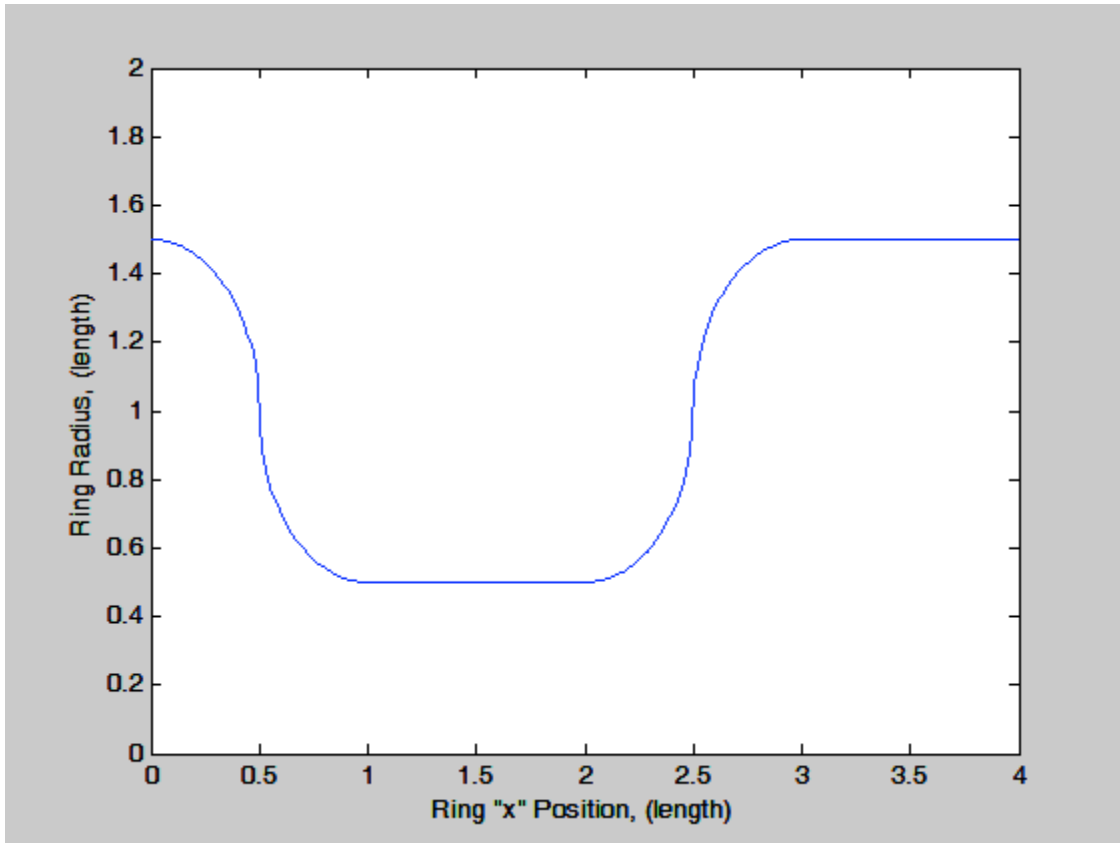


Figure 26. Ring radius versus position for a single ring over a circular cross-section CST.

This information will be useful for design of a future controller based on the position and displacement of the individual ring actuators. A position based controller is often preferable to a force based controller, as position can be easily measured, while force often has to be inferred.

6.3.2 Input Tension Required for the Actuation Rings for the CST Model System

The CST model consists of multiple actuator rings, expanding and contracting over four distinct regions (as defined in Section 6.1). In order to find the output of the entire CST model system, the sum of the force output of each group of active rings must be determined. This will depend on the cross-sectional geometry of the CST, as well as the friction and force output characteristics of the actuators.

The output of the rings in regions I and III can be determined by calculating the force output for each of the rings (using Equations 2 and 3), and summing the results. The output of region II and IV will depend on the interaction between the rings. Again, regions III and IV will

either not be active, as they will be operating in compression, or they will behave the same as regions I and II respectively.

In order to determine the required force input to produce a uniform force output, the required tension input for a unit force output has been plotted in Figure 27. This is the inverse of the mechanical advantage.

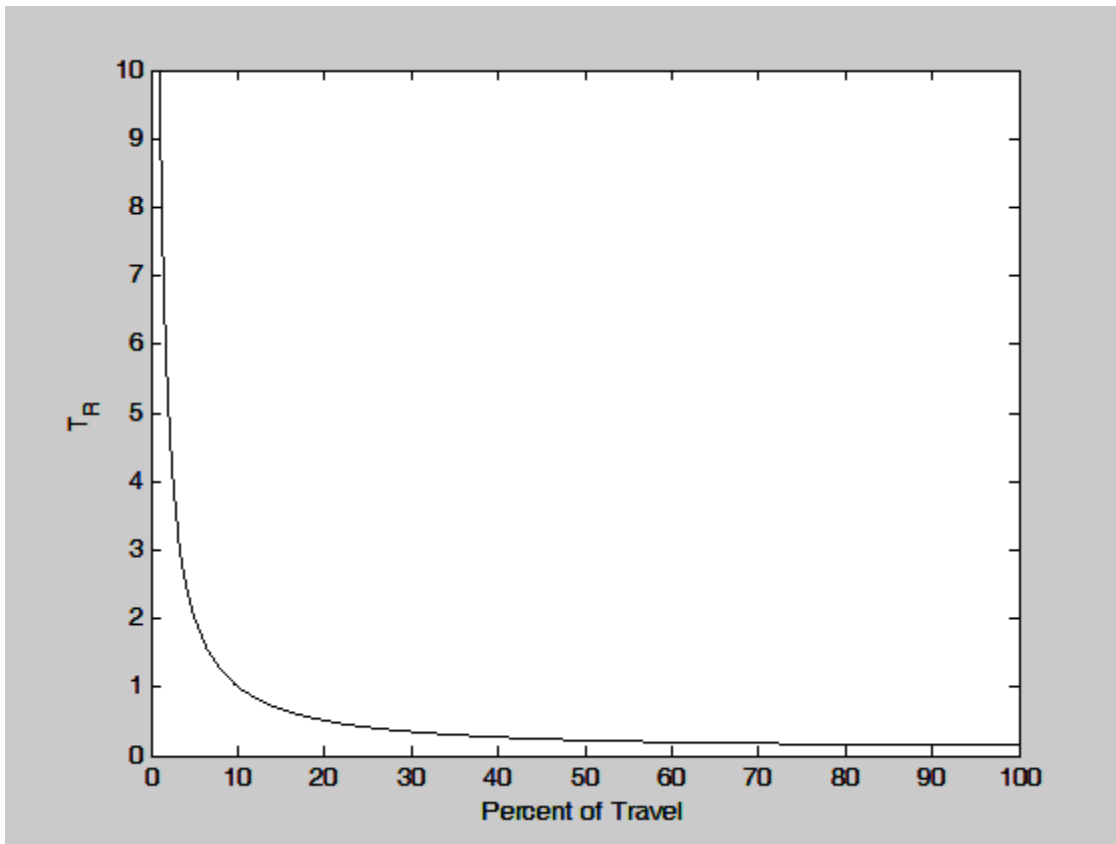


Figure 27. Tension input required in region I, for a unit force output, frictionless.

From this figure it can be seen that in order for a single ring to provide a unit output, a ring just starting to move into region I will require a near infinite force input, as this is because all of the force will be acting in the direction normal to the motion of the skin. As the ring approaches the tip of the CST more of the force is acting in the direction of the skin. A similar pattern can be seen when plotting the required tension input for a pair of rings in region II in Figure 28. Minimal input is required near the tip, increasing as the rings approach the inside inactive region.

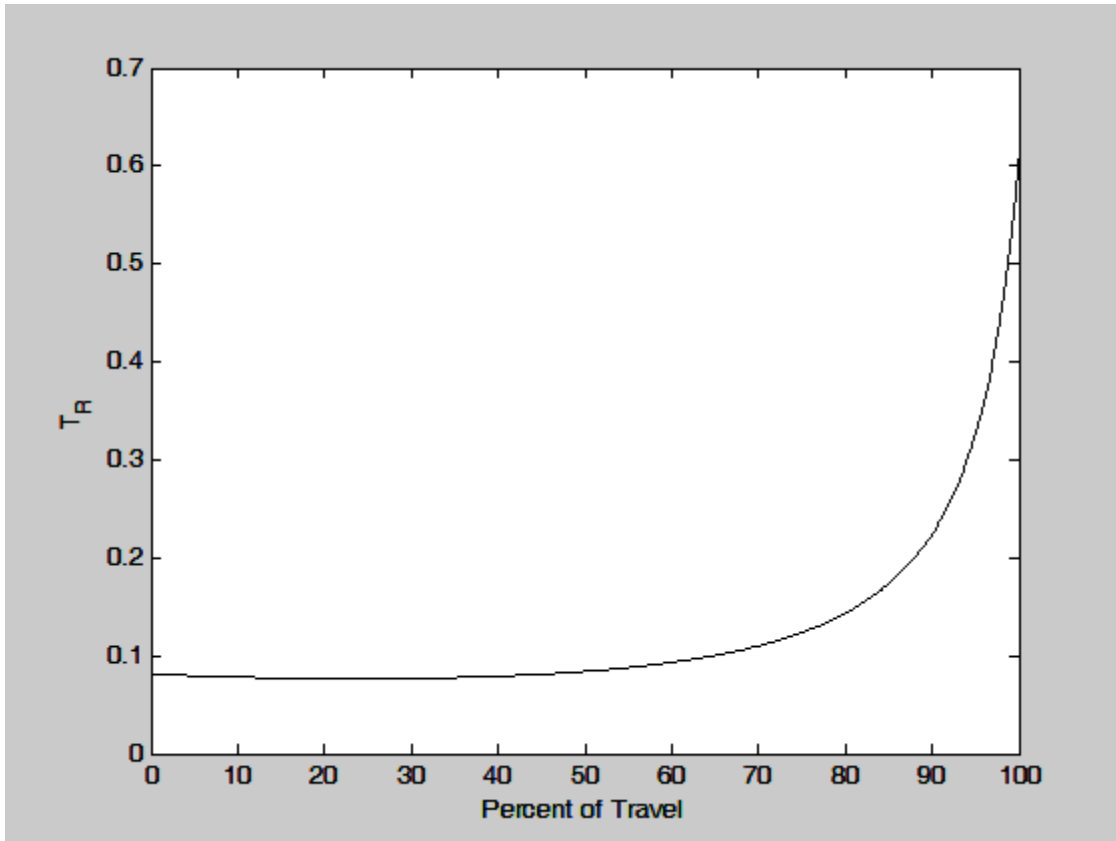


Figure 28. Tension input required for a unit force output.

In order to control the expanding and contacting ring actuators, thought must be given to controlling both the force, and the position of each ring. For example, in this analysis it has been assumed that all of the skin segments connecting the active rings are in tension. If a skin segment were to be in compression the leading rings would be providing no useful force input (if the skin were flexible, and folded) or could be opposing the motion (if the skin were rigid). So ring actuators must follow a position profile as well as a force profile to ensure that all active rings are providing useful force output. A great deal will depend on the characteristics of the actuators and the skin, which is a subject for further research.

Chapter 7

Conclusions and Future Work

The purpose of this research was to investigate a new, fundamental locomotion mechanism based on the motility of monopodial, single-celled organisms, like amoebas. In order to do this the theories of amoeboid motility were studied, and from these the different models for Whole Skin Locomotion were developed. These models are the rear contracting Concentric Solid Tube (CST), the front expanding CST, the wave CST, and the Fluid Filled Toroid (FFT). While these models behave in a similar way to the cytoplasmic streaming in amoebas they are not the same. We are not looking to mimic the amoeba, merely using it for inspiration.

Feasibility experiments were performed using the FFT model. The first experiment was carried out using a pre-tensioned elastic skin, and the second experiment used contracting tension cords. These experiments showed that WSL mechanism is feasible, and with a continuously contracting rear surface it will be able to move continuously.

The CST model was studied in depth, looking at the mechanics of expanding and contracting actuating rings over different regions of the body, and looking at the mechanical advantage and efficiency of different cross-section geometries. From this it was found that the most efficient geometry would be a square cross-section. However, this may not always be the best actuation geometry, as it also has a high mechanical advantage and therefore a short stroke length.

The goal of this research was not to design a Whole Skin Locomotion (WSL) robot, but to develop the mechanics of one of the possible WSL mechanisms, the Concentric Solid Tube (CST) model and its variations. In order to design and build a CST based robot further research must be done on actuators that are capable of acting as expanding and/or contracting rings. Research will also need to be done into skin materials, for the CST analysis it was assumed that the segments connecting the rings were rigid. The advantages and disadvantages of an elastic skin should also be studied. Future work will also include the analysis of the FFT model, which hold great promise, and behave in a unique way.

Whole Skin Locomotion is an entirely new way for robots to move, inspired by the way an amoeba moves. While much work remains before true working prototypes can be built, this

new class of mechanism has great potential for getting robots into unstructured environments such as rubble from a collapsed building, or the inside of the human body.

References

- [1] Laney, D., and Hong, D. W., “Kinematic Analysis of a Novel Rimless Wheel with Independently Actuated Spokes,” 29th ASME Mechanisms and Robotics Conference, Long Beach, California, September 24- September 28, 2005.
- [2] Saranli, U., Buehler, M., and Koditschek, D.E. “RHex: A Simple and Highly Mobile Hexapod Robot,” *International Journal of Robotics Research* 20, July 2001, pp. 616-631.
- [3] Morrey, J. M., Lambrecht, B., Horchler, A. D., Ritzman, R. E., Quinn, R. D., “Highly Mobile and Robust Small Quadruped Robot,” *Proceedings of the 2003 IEEE/RSJ International Conference on Intelligent Robots and Systems*, Las Vegas, NV, Oct. 2003, pp. 82-87.
- [4] Murphy, R. R., “Trial by Fire: Activities of the rescue robots at the World Trade Center from 11-21 September 2001,” *IEEE Robotics and Automation Magazine*, Vol. 11, No. 3, September 2004.
- [5] Blackburn, M. R., Everett, H. R., and Laird, R. T., “After Action Report to the Joint Program Office: Center for the Robotic Assisted Search and Rescue (CRASAR) Related Efforts at the World Trade Center,” *Technical Document 3141*, Space and Naval Warfare Systems Center, San Diego, CA, August 2002.
- [6] Ingram, M. and Hong, D. W., “Whole Skin Locomotion Inspired by Amoeboid Motility Mechanisms”, 29th ASME Mechanisms and Robotics Conference, Long Beach, California, September 24- September 28, 2005.
- [7] Hirose, S. and Fukushima, E.F., “Snakes and Strings: New Robotic Components for Rescue Operations,” *International Journal of Robotics Research*, Vol. 23, No. 4-5, April-May 2004, pp. 341-349.
- [8] Takayama, T., and Hirose, S., “Development of Souryu-I and II,” *Proceedings of the TITech COE/Super Mechano-Systems Symposium*, pp. HRS-1, 2001.
- [9] Kassim, I., Ng, W. S., Feng, G., and Phee, S. J., “Review of Locomotion Techniques for Robotic Colonoscopy,” *Proceedings of the IEEE International Conference on Robotics & Automation*, Taiwan, September 14-19, 2003, pp. 1086 – 1091.
- [10] Phee, S. J., Ng, W. S., Chen, I. M. & Seow-Choen, F., “Development of new locomotive concepts to be used in automation of colonoscopy,” *Proceedings of 9th International Conference for Biomedical Engineering*, Singapore, pp. 87–92, New York, 1997.
- [11] Menciassi, A., Stefanini, C., Gorini, S., Pernorio, G., Kim, B., Park, J. O., and Dario, P., “Locomotion of a Legged Capsule in the Gastrointestinal Tract: Theoretical Study and Preliminary Technological Results,” *Proceedings of the 26th Annual International*

- Conference of the IEEE EMBS, San Francisco, CA, USA, September 1-5, 2004, pp. 2767-2770.
- [12] Hong, D. W., “A Biologically Inspired Whole Skin Locomotion Strategy for Mobile Robots”, US-Korea Conference on Science, Technology and Entrepreneurship (UKC2005), Mechanical Engineering & Robotics Symposium, University of California, Irvine, California, August 11-13, 2005
- [13] Nakabo, Y., Mukai, T., and Asaka, K., “Bio-Mimetic Soft Robots with Artificial Muscles,” SPIE Int. Symp. Smart Materials, Nano- and Micro-Smart Systems, conference, Dec 12 -15, 2004, Australia, Proceedings of SPIE, Vol. 5648, pp. 132 – 144.
- [14] Melhuish, C., Adamatzky, A., Kennedy, B., “Biologically Inspired Robots,” Proceedings of SPIE, Smart Structures and Materials 2002: Electroactive Polymer Actuators and Devices (EAPAD), July 2001, Vol. 4329, pp. 16-27.
- [15] Wingert, A., Lichter, M. D., Dubowsky, S., Hafez, M., “Hyper-redundant robot manipulators actuated by optimized binary-dielectric polymers,” Proceedings of SPIE, Smart Structures and Materials 2002: Electroactive Polymer Actuators and Devices (EAPAD), July 2002, Vol. 4695, pp. 415-423.
- [16] Lackie, J. M., 1986, “Cell Movement and Cell Behavior,” Allen and Unwin, London.
- [17] Allen, R. D., 1973, “Biophysical Aspects of Pseudopodium Formation and Retraction,” The Biology of Amoeba, Ed. Jeon, K. W., Academic Press, Inc., New York and London, pp. 201-247.
- [18] Paljug, E. Ohm, T. Hayati, S., “The JPL Serpentine Robot: a 12-DOF system for inspection,” Proc., 1995 IEEE International Conference on Robotics and Automation, Nagoya, Japan, May 1995.
- [19] Klaassen, B., Paap, K. L., “GMD-SNAKE2: A Snake-Like Robot Driven by Wheels and a Method for Motion Control,” Proceedings of the 1999 IEEE/RSJ International Conference on Intelligent Robots and Systems, Detroit, MI, USA, May, 1999.
- [20] L. Phee, D. Accoto, A. Menciassi, C. Stefanini, M.C. Carrozza, P. Dario, “ Analysis and Development of Locomotion Devices for the Gastrointestinal Tract”, IEEE Transactions on Biomedical Engineering, Vol. 49, No. 6, June 2002.
- [21] Phee, L., Menciassi, A., Gorini, S., Pernorio, G., Arena, A. & Dario, P., “An innovative locomotion principle for minirobots moving in the gastrointestinal tract,” Proceedings of the International Conference on Robotics & Automation, Washington, DC, Vol. 2, pp. 1125–1130, 2002.

- [22] Menciassi, A. and Dario, P., "Bio-inspired solutions for locomotion in the gastrointestinal tract: background and perspectives," *Philosophical Transactions of the Royal Society*, 2003, October Vol. 15, No. 61, pp. 2287-2298.
- [23] Dario, P., Ciarletta, P., Menciassi, A., and Kim, B., 2004 "Modeling and Experimental Validation of the Locomotion of Endoscopic Robots in the Colon," *Int. Jnl. of Robotics Research*, 23, pp. 549-556.
- [24] Slatkin, A.B. Burdick, J. Grundfest, W., "The development of a robotic endoscope," *Proceedings of the 1995 IEEE/RSJ International Conference on Intelligent Robots and Systems*, Pittsburgh, PA , USA, Aug. 1995.
- [25] Roh, S., Choi, H., "Differential-Drive In-Pipe Robot for Moving Inside Urban Gas Pipelines," *IEEE Transactions on Robotics*, vol. 21, issue 1, Feb. 2005, pp. 1–17.
- [26] Breedveld, P., van der Kouwe, D. E., van Gorp, M. A. J., "Locomotion Through the Intestine By Means of Rolling Stents," *Proc. of ASME 2004 Design Engineering Technical Conferences*, Salt Lake City, UT., 2004.
- [27] Flynn A. M., et al., "Tomorrow's Surgery: Micromotors and Microrobots for Minimally Invasive Procedures," *Journal of Minimally Invasive Therapy and Allied Technologies*, Vol. 4, 1998, pp. 343-352.
- [28] Long, G., Anderson, J., and Borenstein, J., "The Kinematic Design of the OmniPede: A New Approach to Obstacle Traversal," *Proc., 2002 IEEE International Conference on Robotics and Automation*, Washington, D.C., pp. 714-719, 2002.
- [29] Schempf, H., "Aurora - Minimalist Design for Tracked Locomotion," *Robotics Research*, R.A. Jarvis and A. Zelinsky (EDs.), Springer Verlag Berlin, 453-465, 2003.
- [30] Allen, R. D., "Motility," *J. Cell Biol.*, 91 (3 Pt 2), pp. 148s-155s, 1981.
- [31] Taylor, D. L., Condeelis, J. S., Moore, P. L., and Allen, R. D., "The Contractile Basis of Amoeboid Movement," *J. Cell Biol.*, 59, pp. 378-394, 1973.
- [32] Lorch, I. J., "Some Historical Aspects of Amoeba Studies," *The Biology of Amoeba*, Ed. Jeon, K. W., Academic Press, Inc., New York and London, pp. 1-36, 1973.
- [33] Ecker, A., "Zur lehre vom bau und leben der contractilen substanz der niedersten thierte," *Z. Wiss. Zool. Abt. A* (abbreviation of: *Zeitschrift fur Zellforschung und mikroskopische Anatomie*), 1, pp. 218-245, 1849.
- [34] Rinaldi, R. and Opas, M., "Graphs of Contracting Glycerinated *Amoeba proteus*," *Nature*, 260, 525-526, 1976.

- [35] Allen, R. D., Cooledge, J. W., and Hall, P. J., "Streaming in cytoplasm dissociated from the giant amoeba, *Chaos chaos*," *Nature*, 187, pp. 896-899, 1960.
- [36] Allen, R. D., Francis, D. W., and Zeh, R., "Direct test of the positive pressure gradient theory of pseudopod extension and retraction in amoebae," *Science*, 174, pp. 1237-1240, 1971.
- [37] Cullen, K. J., and Allen, R. D., "A laser microbeam study of amoeboid movement," *Exp. Cell Res.* 127, pp. 1-10, 1980.
- [38] Pellegrino, S., Keadze, E., Lefort, T., and Watt, A. M., "Low-Cost Hinge for Deployable Structures," Technical Report, University of Cambridge, 2002.
- [39] Yoseph Bar-Cohen (Editor), "Electroactive Polymer (EAP) Actuators as Artificial Muscles: Reality, Potential, and Challenges," Second Edition, SPIE Vol. PM136.
- [40] Cohen, Y., Bao, X., Sherrit, S. & Lih, S. S., "Characterization of the electromechanical properties of ionomeric polymer-metal composites," *Proceedings of SPIE Smart Structures Materials Symp., NDE Conference*, San Diego, CA, March 18–20, 2002, pp. 219–238. Bellingham, WA.
- [41] Bar-Cohen, Y., "EAP History, Current Status, and Infrastructure," *Electroactive Polymer (EAP) Actuators as Artificial Muscles: Reality, Potential, and Challenges*, Bar-Cohen, Y., ed., SPIE – The International Society for Optical Engineering, Bellingham, WA, pp. 3-44, 2001.